Dalton Transactions

ROYAL SOCIETY OF CHEMISTRY

PAPER

View Article Online
View Journal | View Issue

Cite this: *Dalton Trans.*, 2025, **54**, 12667

Analyzing the photophysics and photochemistry of [UO_2(acetylacetonate)$_2$(L)] complexes†

Colin B. Clark, Nora L. Burnett, Alexander N. Ruhren, Eric D. Talbott, Erda Eyubova, Claire Besson, Julien A. Panetier * and John R. Swierk *

Photocatalysis using the uranyl cation, UO_2^{2+}, is underdeveloped. Under visible light illumination, uranyl photocatalysts generate potent excited state oxidants (>2.6 V *vs.* SHE), though the impact of the equatorial ligand environment on the photophysics and photocatalysis of the complexes is poorly understood. To better understand the effect of the equatorial ligands, a series of bis(diketonate) uranyl photocatalysts of the form UO_2(acetylacetonate)$_2$(L) (L = substituted pyridine) were prepared and characterized. The use of electron withdrawing or donating substituents on the pyridine does little to disturb the geometric structure of the complexes, but significant changes in their electronic structure are observed. Specifically, the use of electron-withdrawing cyano- and fluoropyridines increases the ground state reduction potential and weakens the U=O bond. Computational data demonstrates that the ligand-to-metal charge transfer in these complexes involves both the uranium oxo bonds and the acetylacetonate ligand, while the choice of pyridine shifts the absolute energies of the HOMO and LUMO within the complex. Finally, dehydrogenation of 1-phenylethanol was used as a model reaction to explore photochemical reactivity against the performance of uranyl nitrate hexahydrate, the standard choice in uranyl photocatalysis.

Received 19th March 2025,
Accepted 14th July 2025

DOI: 10.1039/d5dt00668f

rsc.li/dalton

Introduction

With the rising cost of metals like ruthenium and iridium, the past two decades have seen an increased interest in the design of photocatalysts that rely on Earth-abundant elements.[1–4] Uranium represents an intriguing, albeit underexplored, alternative to precious metal photocatalysts. The relative abundance of uranium in the Earth's crust is 4 ppm, which is greater than that of molybdenum and tungsten, two elements considered to be earth-abundant.[5] In addition, more than 95% of uranium that has been extracted remains in storage bins outside of enrichment facilities.[3] Most importantly, the main isotope of uranium is ^{238}U, which makes up 99.3% of natural samples, and an even higher proportion of depleted uranium samples. ^{238}U has a long half-life of 4.5 billion years and minimal radioactivity. As a result, while it is a chemical hazard, from a radiological perspective, it is no more dangerous than other heavy metals.[6]

From a photochemical perspective, the uranyl cation (UO_2^{2+}) is particularly intriguing.[7] Formally, UO_2^{2+} features two triply bonded uranium–oxo bonds, generated from the hybridization of the 2p orbitals of O and the 5f/6d orbitals of U. With a bond dissociation energy ~144 kcal mol^{-1}, the oxo groups in UO_2^{2+} are generally deemed to be extremely stable and kinetically inert.[8,9] However, there are few instances where the oxo-groups can be functionalized, with applications concerning uranyl waste management.[10,11] The oxo-groups reside in the axial positions, a structural motif conserved across all UO_2^{2+} complexes. In addition, the large ionic radius of the uranium center allows for great variance in the equatorial ligand environment: the complexes routinely adopt octahedral, pentagonal bipyramidal, or hexagonal bipyramidal geometries with four, five, or six ligands in the equatorial plane, respectively. A trigonal bipyramidal uranyl complex has also been described.[12] However, our understanding of how the equatorial ligand environment alters the photochemical and photophysical properties of the uranyl cation, and thus its reactivity, is not well developed.

The majority of work on photochemical reactivity using UO_2^{2+} complexes relies on uranyl nitrate hexahydrate (**UNH**) as the photocatalyst (Scheme 1).[1,13–21] **UNH** absorbs blue light (400–500 nm) and, like all UO_2^{2+} complexes, undergoes a ligand-to-metal charge transfer (LMCT), creating an oxyl radical. The oxyl radical is highly reactive and exhibits a large reduction potential in the excited state (~2.61 V *vs.* SHE). The excited state reduction potential of **UNH** is comparable to elemental fluorine and higher than most commercially avail-

Binghamton University, Department of Chemistry, Binghamton, NY 13902, USA. E-mail: panetier@binghamton.edu, jswierk@binghamton.edu

†Electronic supplementary information (ESI) available: Crystal structures, NMR data, elemental analysis, computational data, Raman shifts, photochemical reactivity data. CCDC 2430894 and 2447804. For ESI and crystallographic data in CIF or other electronic format see DOI: https://doi.org/10.1039/d5dt00668f

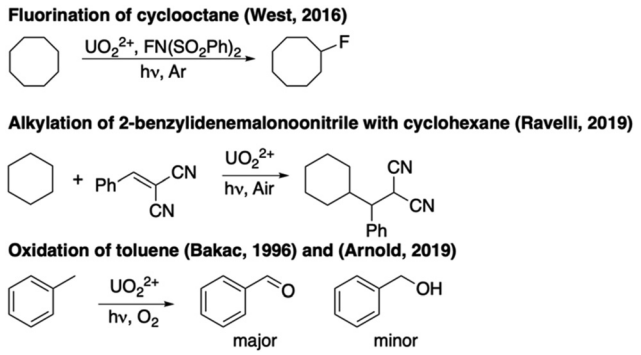

Scheme 1 Select, recent examples of visible light photocatalyzed hydrogen atom transfer using uranyl nitrate hexahydrate (**UNH**) as uranyl source.

able photocatalysts.[22,23] An excited **UNH** complex is capable of hydrogen atom abstraction, resulting in the formal reduction of the uranyl center from U(VI) to U(V).[24] For catalysis to occur, the U(V) species must be oxidized back to U(VI).[14,19] While uranyl photocatalysis has been known for some time, there has been a renewed interest in its use. For example, West and coworkers demonstrated **UNH** could cleave aliphatic C–H bonds when illuminated under blue light, leading to the fluorination of cyclooctane and other unactivated alkanes (*i.e.*, heptane and cyclohexane) in high yields using *N*-fluorobenzenesulfonimide as a fluorinating agent (Scheme 1).[18] Interestingly, the use of uranyl acetate dihydrate as an alternative to **UNH** yielded minimal product. Ravelli and coworkers used **UNH** to cross-couple unactivated (cyclo) alkanes and electrophilic olefins.[14] While Bakac and Mao initially demonstrated that **UNH** could oxidize toluene in the presence of phosphoric acid,[15] Arnold and coworkers more recently improved the yield of oxidized toluene by using a UO_2^{2+} complex bearing a 4,7-diphenyl-1,10-phenanthroline ligand (2% *vs.* 30%).[13] The same complex gave low to moderate yields for the oxidation of other hydrocarbons. Examples of uranyl complexes supported on heterogenous substrates are also known to exhibit good photocatalytic activity.[25–27]

Denning's classic treatment of uranyl photocatalysis assumes the equatorial ligands do not play a role in visible light absorption.[28] However, more recent work calls that assumption into question.[29–32] One gap in the literature on UO_2^{2+} photocatalysts is the lack of studies that systematically vary the equatorial ligands to understand the impact on photophysical and photochemical behavior. Yayamura *et al.* prepared a series of β-diketonate complexes and observed that the lifetime of the complexes followed the Energy Gap Law.[33] Rutkauskaite *et al.* studied several uranyl complexes with substituted phenanthroline ligands, noticing heightened photocatalytic activity when nitrate ions also occupied the equatorial plane as opposed to chloride.[20] Thuéry *et al.* synthesized a series of coordinated polymer complexes, both homo- and heterometallic, with **UNH** being used as a precursor.[34] It was found that for all heterometallic complexes, the solid-state uranyl luminescence was considerably quenched, whereas the homometallic species experienced a pronounced red-shift in the peak emission based on the number of oxygens present on the carboxylate ion ($O_6 \rightarrow O_4$).[39] However, no photocatalytic activity was reported. Other studies involving related UO_2^{2+} photocatalysts have demonstrated varying spectroscopic properties and photocatalytic behaviour, though few insights into how the equatorial ligands impact the electronic structure of the UO_2^{2+} center are reported.[35–39]

To better understand how the equatorial ligand environment impacts the photochemistry of the uranyl cation, in this report we prepare eight uranyl acetylacetonate (acac) complexes with the general form $[UO_2(acac)_2(L)]$ (where L is a substituted pyridine) (Scheme 2). This series of complexes was chosen based on previous work from Kawasaki *et al.*, which described the synthesis and structure of complexes with L as substituted pyridines and imidazole.[40] These complexes are synthetically simple and computationally accessible. The use of a substituted pyridine in the fifth equatorial coordination site offers a simple handle for systematically modulating the electronic environment of the UO_2^{2+} center. Through a combination of spectroscopic, electrochemical, computational, and reactivity studies, we are able to explore how subtle changes in the equatorial ligand environment translate into changes in electronic structure and by extension photocatalytic reactivity.

Experimental

Materials and methods

UNH was purchased from SPI Supplies and used as received. Deuterated acetonitrile and deuterated chloroform were purchased from Oakwood Chemicals and used as received. Acetonitrile was purchased from Thermo Fischer Scientific and dried over 4 Å molecular sieves. All other chemicals were purchased from MilliporeSigma and used as received. We note that while the primary risk with uranyl compounds is its chemical toxicity, ^{238}U is an α emitter and should be handled by trained personnel and with appropriate lab safety precautions.

^1H and ^{13}C Nuclear magnetic resonance spectra were collected using a Bruker Avance III HD 400 MHz instrument and analyzed with Bruker TopSpin software. Spectra for NMR were calibrated using the residual solvent peak.

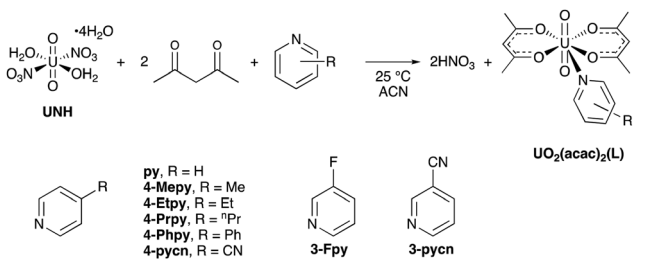

Scheme 2 Synthesis of $[UO_2(acac)_2(L)]$ series.

Elemental analysis was performed by Midwest Microlabs, Inc. (Indianapolis, IA).

General procedure for synthesis and crystallization of uranyl acetylacetonate complexes

$[UO_2(acac)_2(L)]$ complexes were synthesized (Scheme 2) based on the procedure used by Kawasaki *et al.*[40] Briefly, 1 mmol of **UNH** (1 equiv.) was added to 10 mL acetonitrile and allowed to stir. A separate solution of 2 mmol of acetylacetone (2 equiv.) and 1 mmol of the chosen pyridine ligand (1 equiv.) in 5 mL acetonitrile was prepared and allowed to stir. The ligand solution was then added dropwise to the **UNH** solution and stirred for two hours. The solution was then slowly evaporated to dryness at room temperature for several days. The resulting orange powder was thoroughly washed with deionized water and filtered under vacuum, yielding the targeted complex in quantitative yield.

X-ray crystallography

To prepare crystals for X-ray characterization, a saturated solution of $[UO_2(acac)_2(L)]$ was prepared and filtered through a 0.2 μm PTFE syringe filter (ThermoFisher). When acetonitrile was used as the crystallization solvent for $[UO_2(acac)_2(py)]$ and $[UO_2(acac)_2(4\text{-pycn})]$, the solution slowly evaporated for several days until crystals were obtained. When chloroform was used as the crystallization solvent for $[UO_2(acac)_2(4\text{-Mepy})]$, $[UO_2(acac)_2(4\text{-Etpy})]$, and $[UO_2(acac)_2(3\text{-pycn})]$, hexane was added as a counter solvent. After several days, crystals were obtained. A suitable crystal was harvested from the mother liquor and mounted on a 200 μm Mitegen mount. Diffraction data was collected at 296 K on a Rigaku XtaLAB Mini II equipped with a Mo Kα (λ = 0.71073 Å) X-ray source and a hybrid pixel detector, using 0.5° ω and φ scans. CrysAlisPro[41] was used for data reduction and analytical numeric absorption correction[42] using a multifaceted crystal model. The structure was solved using SHELXT[43] and refined with SHELXL[44] using Olex2[45] as interface. Crystallographic data for $[UO_2(acac)_2(4\text{-pycn})]$ and $[UO_2(acac)_2(3\text{-pycn})]$ have been deposited with Cambridge Crystallographic Data Centre and the structures are available at CCDC 2430894 and 2447804,† respectively.

Spectroscopic characterization

Absorption spectra were measured with a Shimadzu UV-2600 UV-Vis Spectrophotometer. Emission spectra were measured with a Shimadzu RF-6000 Spectro Fluorophotometer. For both UV-Vis and fluorometry measurements, samples were prepared in a 1 cm path length optical borosilicate glass cuvette from Starna Cells with a screw top. Samples contained a stirring flea and were placed on a stir plate for 5 minutes in the dark to ensure uniform dispersion of the compounds. Quartz cuvettes were used to measure the absorption spectra at wavelengths shorter than 300 nm while glass cuvettes were used to measure the emission spectra. Raman spectra were obtained with an EZRaman-I Series High Performance Portable Raman Analyzer equipped with a 785 nm laser. Measurements for solid samples were made on a microscopic glass slide, while liquid samples were measured in a glass 2 mL vial.

Relative quantum yields of emission were calculated using degassed tris(2,2′-bipyridine)ruthenium(II) chloride in acetonitrile as a relative standard (Φ = 0.095) according to the method of Arias-Rotondo and McCusker.[46]

Electrochemical characterization

Ground state redox potential measurements were carried out in air. A 4 : 1 solution of acetonitrile to 0.1 M KNO_3 in water served as the supporting electrolyte. Measurements were made with a BioLogic SP-50 potentiostat using a standard three-electrode configuration. The working electrode was a glassy carbon electrode (Pine Research, 0.2 cm^2 surface area), the counter electrode was a platinum wire (MilliporeSigma 99.9%, 0.5 mm diameter), and a single junction Ag/AgCl in 4 M KCl was used as the reference electrode (Pine Research).

Computational methodology

Density functional theory (DFT) calculations were performed with Gaussian 16[47] using the PBE0-D3(BJ) functional.[48] The Stuttgart RLC ECP + valence basis was used for U,[49] and the 6-31G** basis set was employed for all other atoms.[50,51] All calculations were done in acetonitrile (ε = 35.688) using the SMD solvation model.[52] To investigate the excited states of these complexes, time-dependent DFT (TD-DFT) calculations were run using the same level of theory as previously described. The ground-state wavefunctions and natural transition orbitals (NTOs) were visualized using ChimeraX.[53]

General procedure for dehydrogenation of 1-phenylethanol

A 4 mL screw top glass vial was charged with 0.6 mmol of substrate (1 equiv. 0.5 M), 0.06 mmol of uranyl complex (0.10 equiv. 0.05 M), and a stir flea. Acetonitrile was added to achieve a total volume of 1.2 mL. The solution was allowed to stir in the dark for 5 minutes before illumination. For purged reactions, the reaction was capped with a silicone septum (2.5 mm thick) and purged with argon gas for 40 minutes with an outlet needle linked to an oil bubbler. For reactions that were reacting under ambient atmospheric conditions, a silicone/TFE septum (0.060 mm thick) was punctured with a needle to facilitate air flow. Reactions were illuminated in a Penn PhD Photoreactor M2 with a 450 nm light source for the specified period of time. Within the photoreactor, samples were stirred at 500 rpm and were cooled by an internal fan. Yields were calculated *via* quantitative NMR with 100 μL of the illuminated sample, 10 μL of a 1,3-bis(trifluoromethyl)-5-bromobenzene standard, and 390 μL deuterated chloroform.

Results and discussion

Synthesis and structural characterization of complexes

The reaction of **UNH** with Hacac and pyridine derivatives is facile and occurs immediately, accompanied by a distinct color change from greenish yellow for **UNH** to orange for the

$[UO_2(acac)_2(L)]$ complexes. Given the formation of HNO_3 as a by-product of the synthesis, the complexes were washed with water to remove any HNO_3 that was not volatilized. Elemental analysis (ESI†) confirms the lack of HNO_3 in the product. In addition, we note that $[UO_2(acac)_2(L)]$ complexes have much higher solubility in organic solvents (*e.g.*, acetone, acetonitrile, ethyl acetate) than **UNH**.

Crystal structures were collected for five of the complexes to confirm product formation and elucidate any structural changes related to electron donating or withdrawing substituents on the pyridine ligand. Fig. 1 shows the crystal structures for $[UO_2(acac)_2(4\text{-pycn})]$ and $[UO_2(acac)_2(3\text{-pycn})]$, which were previously unreported. Structures for $[UO_2(acac)_2(py)]$, $[UO_2(acac)_2(4\text{-Mepy})]$, and $[UO_2(acac)_2(4\text{-Etpy})]$ were also collected and compared with previously reported structures from Kawasaki (Fig. S1–S3†).[40] Table S2† shows that there is little variance in the U═O bond length as the values range from 1.751(3) Å in the 3-pycn complex to 1.770(4) Å in the 4-pycn complex. The angle between the two uranium oxo bonds shows minimal deviation from linearity. For the py, 4-Etpy, 4-Mepy and 3-pycn complexes the values were 179.4(4)°, 179.0 (4)°, 178.55(14)° and 178.77(15)°, respectively. The largest deviation was seen in the 4-pycn complex, where the OUO angle is 177.1(3)°.

The biggest differences between the complexes were the U–$N_{pyridine}$ bond length and the overall twist angle of the pyridine ligand. The $N_{pyridine}$ length was longest for 4-pycn at a value of 2.665(5) Å and the shortest being py at 2.598(8) Å. The bond length for pyridine ligands is expected to depend mostly on the σ-donating ability of the ligand, with stronger σ donors having a shorter bond length.[54] This would lead to an expected result of the U–$N_{pyridine}$ length being the shortest for 4-Etpy, which was not evident in the crystal structures. This could possibly suggest that some degree of π backbonding to the pyridine is present in the complexes. The relative contribution of the U═O bonding (π_g, π_u) and the non-bonding (δ_u and φ_u) of the uranyl cation to backbonding depends on the twist angle of the pyridine ligand, with only the non-bonding orbitals involved if the twist angle is 90° and only the U═O bonding orbitals involved when the pyridine lies in the equatorial plane. Conversely, these effects could solely be due to the packing of the uranyl complex crystal lattice thus requiring a more future in-depth analysis of the pyridine-uranium bonding through other spectroscopic means.

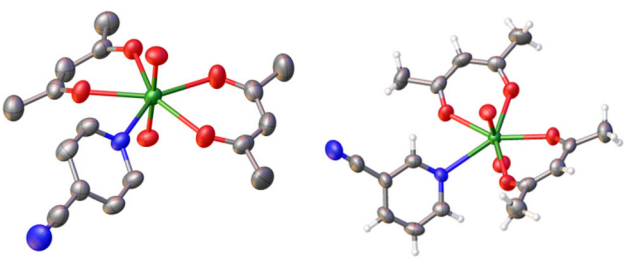

Fig. 1 Crystal structure of $[UO_2(acac)_2(4\text{-pycn})]$ (left) and $[UO_2(acac)_2(3\text{-pycn})]$ (right). Hydrogen atoms have been omitted for clarity. (Carbon = gray, uranium = green, oxygen = red, and nitrogen = blue).

Compared to other uranyl photocatalysts, the structural data does not reveal any clear trends that correlate with reactivity. For example, the U═O bond lengths in **UNH** are 1.770(7) and 1.749(7) Å and the O═U═O bond angle is 179.1(5)°.[55] $[UO_2(Ph_2Phen)(NO_3)_2]$ and $[UO_2Cl_2(Ph_2Phen)]$ exhibit U═O bond lengths of 1.747(3)–1.756(3) Å and 1.746(3)/1.755(3) Å respectively, with O═U═O bond angles of 177° and 178.1(1)°, respectively.[20] These values are consistent with the values in Table S2† for the $[UO_2(acac)_2(L)]$ complexes. We also do not observe any obvious correlations between reactivity and the structural parameters determined from X-ray crystallography (*vide infra*). Broadly speaking, this is consistent with relatively small structural perturbations of uranyl cation by equatorial ligands.[30]

Representative ^1H NMR spectra for $[UO_2(acac)_2]$, $[UO_2(acac)_2(N(CH_3)_3)]$, and $[UO_2(acac)_2(N(C_2H_5)_3)]$ have previously been reported.[56] The ^1H NMR of the complexes we synthesized show that complexation resulted in a marked broadening and a *ca.* 0.30 ppm downfield shift for the acetylacetonate signals, in agreement with the data previously reported for $[UO_2(acac)_2]$, $[UO_2(acac)_2(N(CH_3)_3)]$, and $[UO_2(acac)_2(N(C_2H_5)_3)]$.[56,56,57] As for the pyridine ligands, no clear trend in the chemical shifts was observed. For example, the peaks in $[UO_2(acac)_2(4\text{-Etpy})]$ resulting from the ethyl group exhibit downfield shifts between 0.07 and 0.20 ppm compared to the free ligand. In contrast, the peaks of the pyridine ring exhibit a downfield shift between 0.29 and 0.44 ppm compared to the free ligand, confirming that coordination has a greater impact on the electronic environment of the pyridine hydrogens compared to the pyridine substituent hydrogens. By comparison, the pyridine peaks in $[UO_2(acac)_2(4\text{-Mepy})]$ exhibit shifts of 0.2 and 0.58 ppm. While there is a lack of consistent shift for pyridine peaks, this is expected as the degree of σ-donor and π-backbonding behaviour is likely to differ for each substituted pyridine ligand leading to different NMR shifts.

Importantly, all of pyridinic peaks for the ligands exhibit shifts relative to the free ligand, leading to the conclusion that all of the pyridine ligands are bound to the uranium center.[58,59]

Raman characterization of the complexes (Table S3†) demonstrated a shift of the asymmetric O═U═O stretch to lower wavenumbers when compared to **UNH** (868 cm^{-1}).[13,60,61] Complexes bearing pyridine ligands with electron donating groups exhibited stretches in the range of 824–832 cm^{-1}. In contrast, the complexes with electron-withdrawing ligands (3-pycn, 4-pycn, 3-Fpy) exhibited stretches between 840–866 cm^{-1}. This is consistent with increased σ-donation from pyridine ligands with electron-donating groups.

Electrochemical potentials

Ground state reduction potentials were measured with a three-electrode system. Due to the difference in solubility of **UNH** and the $[UO_2(acac)_2(L)]$ series in organic solvents, a mixed solvent was used, consisting of a 4 : 1 solution of acetonitrile to 0.1 M KNO_3 in water. For **UNH** and the $[UO_2(acac)_2(L)]$ com-

Table 1 U(VI,V) *vs.* SHE potentials for **UNH** and $[UO_2(acac)_2(L)]$ series

$[UO_2(acac)_2(L)]$ L =	U(VI,V) (V *vs.* SHE)
UNH	0.183
3-pycn	0.168
3-Fpy	0.163
4-pycn	0.156
4-Phpy	0.108
4-Etpy	0.057
4-Mepy	0.056
py	0.039
4-Prpy	0.002

plexes, we observe quasi-reversible U(VI,V) peaks. For **UNH**, the half-peak potential was observed at 0.183 V *vs.* SHE (Table 1). This was consistent with previous reports for **UNH**.[14,62,63] For the $[UO_2(acac)_2(L)]$ complexes, the complexes with 3-pycn, 3-Fpy, and 4-pycn exhibited reduction potentials of 0.168, 0.163, and 0.156 V *vs.* SHE, respectively. With more electron-donating substituents, the reduction potential for U(VI,V) shifted to lower potentials between 0.002 and 0.057 V *vs.* SHE, indicating a more electron-rich U(VI) center.

Fig. 2 shows a plot of the U=O Raman stretch *versus* reduction potential. There is a clear relationship between complexes that are more easily reduced, the degree of U=O bond activation, and ligand pK_a. We very clearly observe two regions in Fig. 2, one region with higher pK_a ligands and a lower U=O stretch and a second region with low pK_a ligands and a higher U=O stretch. This also correlates with the reactivity data presented below, where 3-pycn, 3-Fpy, and 4-pycn exhibit better photochemical reactivity than the other $[UO_2(acac)_2(L)]$ complexes.

Photophysical characterization of complexes

As noted above, complexation to acac and pyridine ligands results in a noticeable change in color in the $[UO_2(acac)_2(L)]$ complexes. The electronic absorbance spectrum of **UNH** has

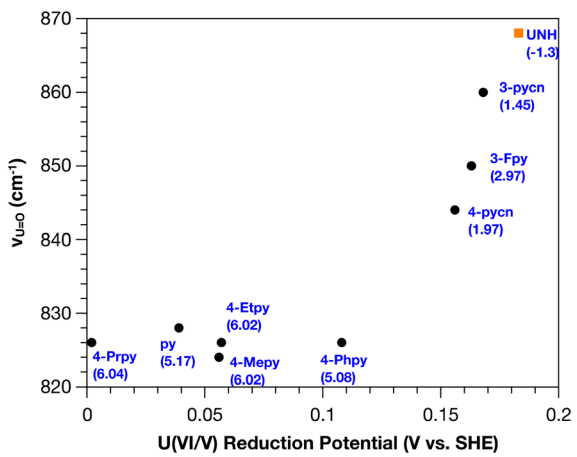

Fig. 2 Plot of U=O Raman stretch *versus* U(VI/V) reduction potential for $[UO_2(acac)_2(L)]$ complexes (black circles) and **UNH** (orange square). Pyridine ligand and pK_a for protonated ligand in blue. For **UNH** the pK_a of nitric acid was used.

multiple peaks spanning from the blue light region to the Ultraviolet A (UVA) region (356 nm) with a maximum at 423 nm (~10 M^{-1} cm^{-1}) (Fig. S52†). In contrast, all of the $[UO_2(acac)_2(L)]$ complexes exhibit two distinct LMCT peaks at ~450 nm and ~370 nm (Fig. S53†). Molar absorptivity constants in the visible region are on the order of 100 to 200 M^{-1} cm^{-1}, which is roughly one order of magnitude higher than **UNH** (Table 1). We also observed a modest hypochromic shift going from pyridine ligands with electron-withdrawing groups to electron-donating groups, with the shift occurring for both visible and UV peaks. Compared to **UNH**, the $[UO_2(acac)_2(L)]$ complexes are very weakly emissive (Table 2). Emission quantum yields from $[UO_2(acac)_2(L)]$ complexes were on the order of 10^{-5} to 10^{-6}, compared to 2.95×10^{-2} for **UNH**. We were unable to determine excited state lifetimes for the $[UO_2(acac)_2(L])$ complexes. However, Yayamura *et al.* reported an emissive lifetime of 900 ps for $[UO_2(acac)_2(THF)]$, which was ascribed to a small $E_{0,0}$ gap and strong deactivating vibration.[33] However, the $E_{0,0}$ for the $[UO_2(acac)_2(L)]$ complexes is approximately 1.92×10^4 cm^{-1}, which, based on Yayamura's data, would be predicted to give a longer emission lifetime and higher emission quantum yield.[33]

Computational results

We performed DFT calculations to generate optimized structures and wavefunctions for each of the $[UO_2(acac)_2(L)]$ complexes. The computed bond angles and distances agree with the experimentally determined X-ray crystallographic structures (Tables S4–S6†). Specifically, the O=U=O bond angles of ~180° and U=O bond lengths of ~1.7 Å are consistent for all $[UO_2(acac)_2(L)]$ complexes, as well as **UNH**.

In order to investigate the excited states of the complexes, we turned to TD-DFT. For the sake of brevity, only the results related to $[UO_2(acac)_2(py)]$ will be discussed in detail. Additional information about the other complexes can be found in the ESI.† As shown in Fig. 3, the calculated and experimental UV-Vis spectra for $[UO_2(acac)_2(py)]$ are in excellent agreement with each other. Importantly, the calculations correctly predict the experimentally observed visible light transitions around 460 nm. Notably, calculations for **UNH** do not indicate any visible light transitions, suggesting those may be spin-forbidden, consistent with the low molar extinction coeffi-

Table 2 Peak wavelengths (λ) and molar absorptivity constants (ε) of $[UO_2(acac)_2(L)]$ series within the visible and UV regions

$[UO_2(acac)_2(L)]$ L =	$\lambda_{max,\,abs}$ (nm)	ε_{max} (M^{-1} cm^{-1})	$\lambda_{max,\,em}$ (nm)	Φ
UNH	356, 423	5, 10	505	2.95×10^{-2}
py	366, 445	1440, 171	520	1.05×10^{-5}
4-Mepy	368, 445	1269, 218	520	1.41×10^{-5}
4-Etpy	367, 447	1293, 234	519	8.14×10^{-6}
4-Prpy	367, 445	1256, 203	521	1.80×10^{-5}
4-Phpy	367, 445	1015, 171	521	3.33×10^{-5}
3-Fpy	369, 450	1239, 231	517	1.45×10^{-4}
3-pycn	372, 451	458, 91	521	8.07×10^{-5}
4-pycn	370, 451	700, 146	520	3.23×10^{-5}

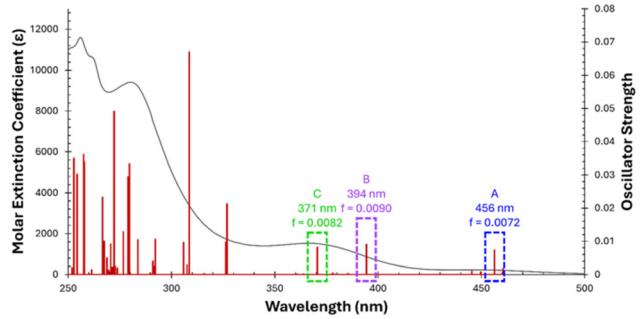

Fig. 3 Experimental (gray) and calculated (red) UV-Vis spectra for $[UO_2(acac)_2(py)]$. The experimental spectrum is given in molar absorptivity (L mol^{-1} cm^{-1}) while the calculated spectrum is displayed using the oscillation strength of the selected transitions.

cients in **UNH**. Calculations for the other $[UO_2(acac)_2(L)]$ complexes produced a similar agreement between the predicted and experimental absorption spectra. Natural transition orbitals (NTOs) for $[UO_2(acac)_2(py)]$ were generated and visualized for the predicted transitions at 456, 394, and 371 nm (Fig. 4) to better understand the nature of the electronic transition. The NTOs in the visible region describe a ligand-to-metal charge transfer (LMCT) transition that includes contributions from both the acac and oxo ligands to the uranium center. Classic descriptions of uranyl light absorption assume no contribution from the equatorial ligands, but that is clearly not the

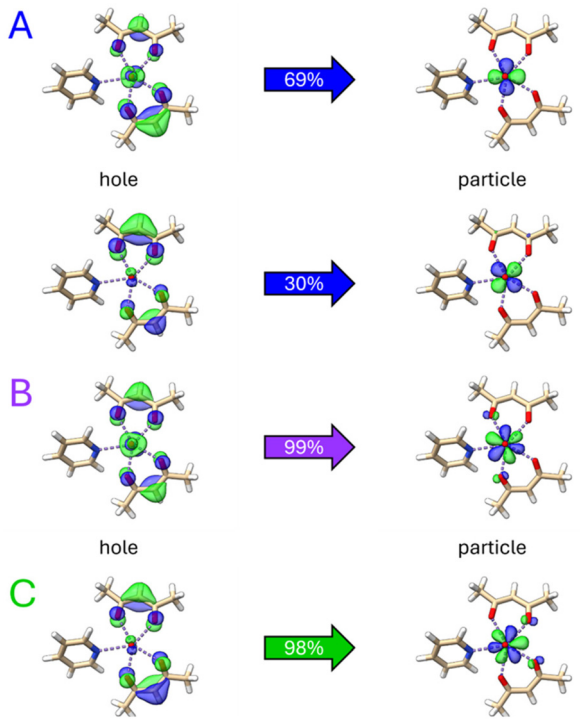

Fig. 4 NTOs for the calculated transitions at (A) 456, (B) 394, and (C) 371 nm in Fig. 3. In (A) the overall transition was made up of two separate contributions, both of which depict a ligand-to-metal charge transfer (LMCT).

case with $[UO_2(acac)_2(L)]$ complexes. The calculations also indicate little to no contribution from the pyridine ligand.

In an attempt to understand the contribution of the pyridine ligand to the electronic structure of the $[UO_2(acac)_2(L)]$ complexes, molecular orbitals (MOs) and molecular orbital diagrams were calculated for all of the complexes (Fig. 5 and Fig. S65–71†). The highest occupied molecular orbital (HOMO) energy, the lowest unoccupied molecular orbital (LUMO) energy, as well as ±10 MO energies were all calculated and visualized in ChimeraX.[53] Selected orbitals' energies and corresponding MOs for $[UO_2(acac)_2(py)]$ are shown in Fig. 5. The calculated HOMO/LUMO gap was 3.92 eV, which was consistent with an average HOMO/LUMO gap of 3.92 eV for the rest of the $[UO_2(acac)_2(L)]$ complexes (Fig. 6). We observed that the HOMO for $[UO_2(acac)_2(py)]$ and other $[UO_2(acac)_2(L)]$ complexes was predominantly localized on the carbon atoms of the acac backbone. Using population analyses, these carbon atoms comprise about 50% of the overall electron density for each species' HOMO. The remaining contribution to the electron density for the HOMO was primarily from the acac oxygen atoms. The LUMO, meanwhile, was composed of around 90% uranium 5f-orbital. This was true for all of the complexes. LUMO+1 and LUMO+2 shared the same 90% contribution from the uranium f-orbital, with one exception. In $[UO_2(acac)_2(4\text{-pycn})]$, the LUMO+2 had only a 46% contribution from the uranium f-orbital. The remaining electron density is from the pyridine ligand, namely the carbon at the *para*-position. This contribution was 10%, with the remaining contribution coming from the other atoms within the pyridine ligand.

Comparison of the MO diagram across multiple complexes begins to reveal the impact of the pyridine ligand. Fig. 6 demonstrates that while the HOMO/LUMO gap is relatively consistent, the absolute position of the HOMO and LUMO do shift depending on the pyridine ligand. There is a 20 meV shift to lower energy in the HOMO position going from 4-Etpy to 4-pycn, and a 60 meV shift in the LUMO energy. Taking the comparison between the $[UO_2(acac)_2(py)]$ and $[UO_2(acac)_2(3\text{-pycn})]$ complexes, the more electron-withdrawing pyridine results in more MOs with primarily pyridine ligand character. This could offer some insight into the reactivity of these complexes, though further computational analysis is required and is currently underway.

Photochemical reactivity

Having explored the photophysical and electronic structure of the complexes, we next turned to reactivity studies. We focused on dehydrogenation as a model reaction for uranyl HAT reactivity. Dehydrogenation is a valuable process for synthetic applications and the production of molecular hydrogen has applications in solar energy storage.[64–66] We selected 1-phenylethanol as a low-volatility model substrate for dehydrogenation. Using **UNH**, we identified optimum reaction conditions as being 10 mol% catalyst loading in acetonitrile under an air atmosphere, which gave an 84 ± 4% yield for acetophenone after 24 hours (Table S16†). We note that the reaction is photo-

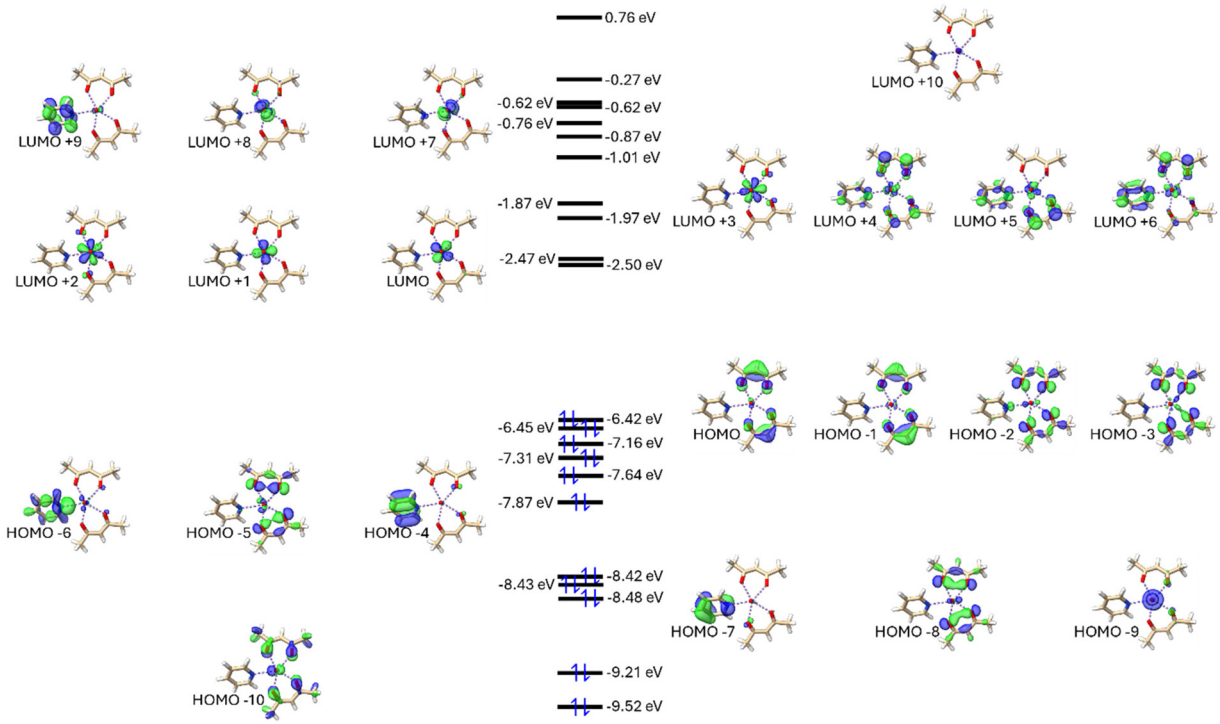

Fig. 5 Selected MOs for $[UO_2(acac)_2(py)]$. The HOMO/LUMO gap is 3.92 eV.

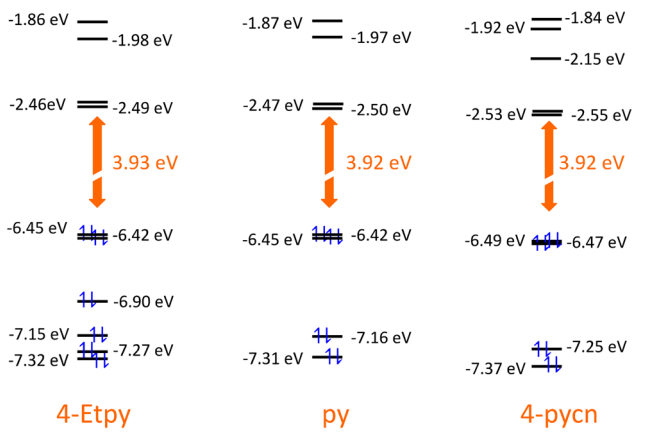

Fig. 6 Selected MO energies for $[UO_2(acac)_2(4\text{-Etpy})]$, $[UO_2(acac)_2(py)]$, and $[UO_2(acac)_2(4\text{-pycn})]$ complexes. The HOMO/LUMO gaps are shown in orange.

Table 3 Photocatalytic dehydrogenation of 1-phenylethanol to acetophenone with **UNH** and $[UO_2(acac)_2(L)]$ complexes at 24 and 48 h. Reaction yields are calculated with an average of three trials when standard deviation is provided

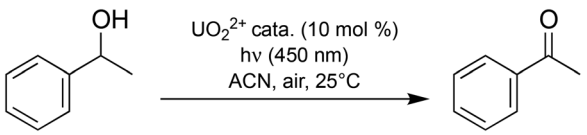

Entry	$[UO_2(acac)_2(L)]$ L =	24 h yield (%)	48 h Yield (%)
1	**UNH**	84 ± 4	98
2	py	22 ± 2	40
3	4-Mepy	8 ± 1	21
4	4-Etpy	22 ± 1	42
5	4-Prpy	16 ± 1	52
6	4-Phpy	15 ± 2	92
7	3-Fpy	67 ± 5	96
8	3-pycn	77 ± 3	99
9	4-pycn	70 ± 4	95

catalytic, as no product is observed without the presence of the photocatalyst or when the reaction was carried out in the dark.

Using the optimized conditions developed with **UNH**, we next explored the reactivity of the $[UO_2(acac)_2(L)]$ complexes. While most of the complex exhibited decreased reactivity compared to **UNH**, complexes bearing electron-withdrawing functional groups exhibited comparable yields to **UNH** (Table 3). Specifically, $[UO_2(acac)_2(3\text{-pycn})]$ (entry 8) had the greatest yield out of the series after 24 hours of illumination with an acetophenone yield of 77 ± 3%, which is within the error of the performance of **UNH**. Over a 48 hour period, **UNH** and the three complexes containing cyano- or fluoropyridine achieved nearly complete conversion of 1-phenylethanol to acetophenone.

When the same reaction was tested in chloroform, a more non-polar solvent (compared to acetonitrile), we observed increased solubility of the $[UO_2(acac)_2(L)]$ series relative to **UNH**. Overall, dehydrogenation reactivity decreased for all uranyl complexes (including **UNH**), in chloroform (Table S17†). Interestingly, we found that $[UO_2(acac)_2(3\text{-Fpy})]$ surpassed the performance of

UNH (38 ± 3% *vs.* 29 ± 2%), unlocking the potential to expand the scope of uranyl photoreactivity in less polar solvents that may be desirable for synthetic utility.

While we have yet to carry out detailed mechanistic studies, we hypothesize that the excited uranyl photocatalyst abstracts the hydrogen from the carbon bearing the hydroxyl group to generate a carbon-centered radical and U(v) species, $U(O)OH^+$. The second HAT from oxygen may be accomplished thermally or *via* a second photoinduced HAT step. Finally, we propose that O_2 from air oxidizes the U(v) species back to U(vi), which may be accompanied by the formation of H_2O_2. We note that under inert atmosphere (Table S18†), the reaction yields are notably decreased for all uranyl photocatalysts and that a black precipitate forms. We hypothesize that in the absence of O_2, U(v) can undergo disproportionation to form U(iv) and U(vi) species.[67,68] U(iv) species are known to form insoluble precipitates,[69,70] leading to a loss of reactivity. Finally, we carried out dehydrogenation of 1-phenylethanol by $[UO_2(acac)_2(3\text{-pycn})]$ with excess 3-pycn present and observed no change in yield. This suggests that loss of the pyridine ligand is not part of the mechanism.

Conclusions

The $[UO_2(acac)_2(L)]$ complexes in this report represent a simple platform for exploring the impact of the equatorial ligands on the electronic structure, photophysical, and photocatalytic properties of the complexes. Subtle modification of the pyridine ligand leads to measurable changes in spectroscopic and redox properties and significant differences in photocatalytic activity. Computational studies are able to rationalize these differences, with the acac ligands participating in the LMCT transition and the pyridine ligands shifting the absolute potentials of energy levels within the complex.

Intriguingly, the separate effects of the acac and pyridine ligands suggest that light harvesting and property tuning can be decoupled into different ligands in uranyl photocatalysts. Acac is just the simplest example of a rich family of diketonate and related derivatives, which could be leveraged to provide broader insights into how light absorption is further impacted. Likewise, extension to other N- or O-heterocycles may offer opportunities for more significant changes to the uranyl electronic structure.

Finally, though the focus of this report is not synthetic utility, it should be noted that $[UO_2(acac)_2(L)]$ complexes with electron-withdrawing ligands (cyanopyridine, fluoropyridine) achieve comparable photocatalytic reactivity to **UNH**, which is typically the standard uranyl complex used in synthetic applications. Notably, $[UO_2(acac)_2(3\text{-Fpy})]$ surpassed **UNH**'s reactivity in chloroform. All of the $[UO_2(acac)_2(L)]$ complexes exhibit high solubility in organic solvents that are inaccessible to **UNH** or other uranyl photocatalysts (*e.g.*, $[UO_2(Ph_2Phen)(NO_3)_2]$), which suggests that $[UO_2(acac)_2(L)]$ complexes may also represent a pathway towards broader synthetic utility for uranyl photocatalysis.

Author contributions

Colin B. Clark: conceptualization (supporting); investigation (equal); formal analysis (equal); writing – original draft (lead); writing – review and editing (equal). Nora L. Burnett: investigation (equal); formal analysis (equal); writing – original draft (supporting); writing – review and editing (equal). Alexander N. Ruhren: investigation (supporting); formal analysis (supporting); writing – original draft (supporting); writing – review and editing (equal). Eric D. Talbott: investigation (supporting); formal analysis (supporting); writing – original draft (supporting); writing – review and editing (supporting). Erda Eyubova: formal analysis (supporting); writing – original draft (supporting). Claire Besson: formal analysis (supporting); writing – review and editing (equal). Julien A. Panetier: formal analysis (supporting); writing – review and editing (equal); supervision (equal). John R. Swierk: conceptualization (lead); formal analysis (equal); writing – original draft (supporting); writing – review and editing (equal); supervision (equal); project administration (lead); funding (lead).

Conflicts of interest

There are no conflicts to declare.

Data availability

The data supporting this article have been included as part of the ESI.†

Acknowledgements

NLB and JRS thank Maksim Livshits for helpful discussions. The authors gratefully acknowledge the financial assistance provided for this publication through the generosity of donors to the Harpur College Advocacy Council Faculty Development Endowment—an endowed fund that invests deeply in the research, creative activities, and professional development of Harpur College of Arts and Sciences faculty at Binghamton University. EDT would like to thank the Arnold and Mabel Beckman Foundation for funding through the Beckman Scholars Program.

References

1 N. Behera and S. Sethi, Unprecedented Catalytic Behavior of Uranyl(VI) Compounds in Chemical Reactions, *Eur. J. Inorg. Chem.*, 2021, (2), 95–111, DOI: 10.1002/ejic.202000611.
2 A. R. Fox, S. C. Bart, K. Meyer and C. C. Cummins, Towards Uranium Catalysts, *Nature*, 2008, **455**(7211), 341–349, DOI: 10.1038/nature07372.

3 D. Hu and X. Jiang, Perspectives for Uranyl Photoredox Catalysis, *Synlett*, 2021, (13), 1330–1342, DOI: 10.1055/a-1493-3564.
4 H. D. Burrows and T. J. Kemp, The photochemistry of the uranyl ion, *Chem. Soc. Rev.*, 1974, **3**, 139–165, DOI: 10.1039/CS9740300139.
5 L. Alig, M. Fritz and S. Schneider, First-Row Transition Metal (De)Hydrogenation Catalysis Based On Functional Pincer Ligands, *Chem. Rev.*, 2019, **119**(4), 2681–2751, DOI: 10.1021/acs.chemrev.8b00555.
6 Uranium and Depleted Uranium – World Nuclear Association. https://world-nuclear.org/infoormation-library/nuclear-fuel-cycle/uuranium-resources/uranium-and-deplleted-uranium (accessed 2025-03-13).
7 B. E. Cowie, J. M. Purkis, J. Austin, J. B. Love and P. L. Arnold, Therman and Photochemical Reduction and Functionalization Chemistry of the Uranyl Dication $[U^{VI}O_2]^{2+}$, *Chem. Rev.*, 2019, **119**(18), 10595–10637, DOI: 10.1021/acs.chemrev9b00048.
8 P. L. Arnold, A.-F. Pécharman, E. Hollis, A. Yahia, L. Maron, S. Parsons and J. B. Love, Uranyl Oxo Activation and Functionalization by Metal Cation Coordination, *Nat. Chem.*, 2010, **2**(12), 1056–1061, DOI: 10.1038/nchem.904.
9 B. E. Cowie, G. S. Nichol, J. B. Love and P. L. Arnold, Double Uranium Oxo Cations Derived from Uranyl by Borane or Silane Reduction, *Chem. Commun.*, 2018, **54**(31), 3839–3842, DOI: 10.1039/C8CC00341F.
10 R. J. Baker, New Reactivity of the Uranyl(VI) Ion, *Chem. – Eur. J.*, 2012, **18**, 16258–16271, DOI: 10.1002/chem.201203085.
11 S. Fortier and T. W. Hayton, Oxo ligand functionalization in the uranyl ion (UO_2^{2+}), *Coord. Chem. Rev.*, 2010, **254**(3–4), 197–214, DOI: 10.1016/j.ccr.2009.06.003.
12 P. Thuéry, M. Nierlich, B. Masci, B. Asfari and J. Vicens, An unprecedented trigonal coordination geometry for the uranyl ion in its complex with p-tert-butylhexahomotrioxacalix[3]arene, *J. Chem. Soc., Dalton Trans.*, 1999, **18**, 3151–3152, DOI: 10.1039/A905939C.
13 P. L. Arnold, J. M. Purkis, R. Rutkauskaite, D. Kovacs, J. B. Love and J. Austin, Controlled Photocatalytic Hydrocarbon Oxidation by Uranyl Complexes, *ChemCatChem*, 2019, **11**(16), 3786–3790, DOI: 10.1002/cctc.201900037.
14 L. Capaldo, D. Merli, M. Fagnoni and D. Ravelli, Visible Light Uranyl Photocatalysis: Direct C–H to C–C Bond Conversion, *ACS Catal.*, 2019, **9**(4), 3054–3058, DOI: 10.1021/acscatal.9b00287.
15 Y. Mao and A. Bakac, Photocatalytic Oxidation of Toluene to Benzaldehyde by Molecular Oxygen, *J. Phys. Chem.*, 1996, **100**(10), 4219–4223, DOI: 10.1021/jp9529376.
16 Y. Mao and A. Bakac, Uranyl-Sensitized Photochemical Oxidation of Naphthalene by Molecular Oxygen, Role of Electron Transfer, *J. Phys. Chem. A*, 1997, **101**(43), 7929–7933, DOI: 10.1021/jp962961z.
17 W.-D. Wang, A. Bakac and J. H. Espenson, Uranium(VI)-Catalyzed Photooxidation of Hydrocarbons with Molecular Oxygen, *Inorg. Chem.*, 1995, **34**(24), 6034–6039, DOI: 10.1021/ic00128a014.
18 J. G. West, T. A. Bedell and E. J. Sorensen, The Uranyl Cation as a Visible–Light Photocatalyst for $C(sp^3)$–H Fluorination, *Angew. Chem., Int. Ed.*, 2016, **55**(31), 8923–8927, DOI: 10.1002/anie.201603149.
19 J. Yu, C. Zhao, R. Zhou, W. Gao, S. Wang, K. Liu, S. Chen, K. Hu, L. Mei, L. Yuan, Z. Chai, H. Hu and W. Shi, Visible–Light–Enabled C–H Functionalization by a Direct Hydrogen Atom Transfer Uranyl Photocatalyst, *Chem. – Eur. J.*, 2020, **26**(69), 16521–16529, DOI: 10.1002/chem.202003431.
20 R. Rutkauskaite, X. Zhang, A. W. Woodward, Y. Liu, G. Herrera, J. Purkis, S. D. Woodall, M. Sarsfield, G. Schreckenbach, L. S. Natrajan and P. L. Arnold, The Effect of Ancillary Ligands on Hydrocarbon C–H Bond Functionalization by Uranyl Photocatalysts, *Chem. Sci*, 2024, **15**(18), 6965–6978, DOI: 10.1039/D4SC01310G.
21 Uranyl nitrate. American Chemical Society. https://www.acs.org/molecule-of-the-week/archive/u/uranyl-nitrate.html (accessed 2025-02-25).
22 S. Gary, M. Landry and S. Bloom, Spectral and Electrochemical Properties of Common Photocatalysts in Water: A Compendium for Aqueous Photoredox Catalysis, *Synlett*, 2023, (16), 1911–1914, DOI: 10.1055/a-2097-1051.
23 D. A. DiRocco, in *Electrochemical Series of Photocatalysts and Common Organic Compounds*, 2014.
24 L. S. Natrajan, Developments in the photophysics and photochemistry of actinide ions and their coordination compounds, *Coord. Chem. Rev.*, 2012, **256**, 1583–1603, DOI: 10.1016/j.ccr.2012.03.029.
25 Y. Li, J. Su, E. Mitchell, G. Zhang and J. Li, Photocatalysis with visible-light-active uranyl complexes, *Sci. China: Chem.*, 2013, **56**, 1671–1681, DOI: 10.1007/s11426-013-4965-y.
26 P. A. Kolinko, T. N. Filippov, D. V. Kozlov and V. Parmon, Ethanol vapor photocatalytic oxidation with uranyl modified titania under visible light: Comparison with silica and alumina, *J. Photochem. Photobiol., A*, 2012, **250**, 72–77, DOI: 10.1016/j.jphotochem.2012.09.015.
27 V. Krishna, V. S. Kamble, N. M. Gupta and P. Selvam, Uranyl-Anchored MCM-41 as a Highly Efficient Photocatalyst in the Oxidative Destruction of Short Chain Linear Alkanes: An in situ FTIR Study, *J. Phys. Chem. C*, 2008, **112**, 15832–15843, DOI: 10.1021/jp802779e.
28 R. G. Denning, Electronic Structure and Bonding in Actinyl Ions and their Analogs, *J. Phys. Chem. A.*, 2007, **111**, 4125–4143, DOI: 10.1021/jp071061n.
29 P. Di Pietro and A. Kerridge, U–Oyl Stretching Vibrations as a Quantitative Measure of the Equatorial Bond Covalency in Uranyl Complexes: A Quantum-Chemical Investigation, *Inorg. Chem.*, 2016, **55**, 573–583, DOI: 10.1021/acs.inorgchem.5b01219.
30 S. Fortier and T. W. Hayton, Oxo ligand functionalization in the uranyl ion (UO_2^{2+}), *Coord. Chem. Rev.*, 2010, **254**, 197–214, DOI: 10.1016/j.ccr.2009.06.003.
31 D. E. Morris, Redox Energetics and Kinetics of Uranyl Coordination Complexes in Aqueous Solution, *Inorg. Chem.*, 2002, **41**, 3542–3547, DOI: 10.1021/ic0201708.

32 J. Su, K. Zhang, W. H. E. Schwarz and J. Li, Uranyl-Glycine-Water Complexes in Solution: Comprehensive Computational Modeling of Coordination Geometries, Stabilization Energies, and Luminescence Properties, *Inorg. Chem.*, 2011, **50**, 2082–2093, DOI: 10.1021/ic200204p.

33 T. Yayamura, S. Iwata, S.-I. Iwamura and H. Tomiyasu, Effect of complexation on the excited state of uranyl β-diketonato complexes: applications of the energy gap law, *J. Chem. Soc., Faraday Trans.*, 1994, **90**, 3253–3259, DOI: 10.1039/FT9949003253.

34 P. Thuéry and J. Harrowfield, Structural Consequences of 1,4-Cyclohexanedicarboxylate Cis/Trans Isomerism in Uranyl Ion Complexes: From Molecular Species to 2D and 3D Entangled Nets, *Inorg. Chem.*, 2017, **56**, 13464–13481, DOI: 10.1021/acs.inorgchem.7b02176.

35 Q. Zhang, B. Jin, R. Peng, X. Wang, Z. Shi, Q. Liu, S. Lei and H. Liang, Investigation on the Synthesis and Photocatalytic Property of Uranyl Complexes of the β-Diketonates Biscatecholamide Ligand, *Int. J. Photoenergy*, 2017, 8041647, DOI: 10.1155/2017/8041647.

36 J. He, X. Gong, Y. Li, Q. Zhao and C. Zhu, Synthesis and Photocatalytic sp^3 C-H Bond Functionalization of Salen-Ligand-Supported Uranyl(VI) Complexes, *Molecules*, 2024, **29**, 4077, DOI: 10.3390/molecules29174077.

37 M. Azam, S. I. Al-Resayes, G. Velmurugan, P. Venuvanalingam, J. Wagler and E. Kroke, Novel Uranyl (VI) Complexes Incorporating Propylene-Bridged Salen-Type N_2O_2-Ligands: A Structural and Computational Approach, *Dalton Trans.*, 2014, **44**(2), 568–577, DOI: 10.1039/C4DT02112F.

38 M. Azam, G. Velmurugan, S. M. Wabaidur, A. Trzesowska-Kruszynska, R. Kruszynski, S. I. Al-Resayes, Z. A. Al-Othman and P. Venuvanalingam, Structural Elucidation and Physicochemical Properties of Mononuclear Uranyl(VI) Complexes Incorporating Dianionic Units, *Sci. Rep.*, 2016, **6**(1), 32898, DOI: 10.1038/srep32898.

39 M. P. Redmond, S. M. Cornet, S. D. Woodall, D. Wittaker, D. Collison, M. Helliwelll and L. S. Natrajan, Probing the local coordination environment and nuclearity of uranyl (VI) complexes in non-aqueous media by emission spectroscopy, *Dalton Trans.*, 2011, **40**, 3914–3926, DOI: 10.1039/c0dt01464h.

40 T. Kawasaki, T. Nishimura and T. Kitazawa, Uranyl(VI)–Acetylacetonate Coordination Compounds with Various N Heterocyclic Ligands, *Bull. Chem. Soc. Jpn.*, 2010, **83**(12), 1528–1530, DOI: 10.1246/bcsj.20100159.

41 CrysAlisPro 1.171.43.120a (Rigaku OD, 2024).

42 R. C. Clark and J. S. Reid, The analytical calculation of absorption in multifaceted crystals, *Acta Crystallogr. A*, 1995, **51**, 887–897, DOI: 10.1107/S0108767395007367.

43 G. M. Sheldrick, SHELXT – Integrated space-group and crystal-structure determination, *Acta Crystallogr. A*, 2015, **71**, 3–8, DOI: 10.1107/S2053273314026370.

44 G. M. Sheldrick, Crystal structure refinement with SHELXL, *Acta Crystallogr. C*, 2015, **71**, 3–8, DOI: 10.1107/S2053229614024218.

45 O. V. Dolomanov, L. J. Bourhis, R. J. Gildea, J. A. K. Howard and H. Puschmann, OLEX2: A complete structure solution, refinement and analysis program, *J. Appl. Crystallogr.*, 2009, **42**, 339–341, DOI: 10.1107/S0021889808042726.

46 D. M. Arias-Rotondo and J. K. McCusker, The Photophysics of Photoredox Catalysis: A Roadmap for Catalyst Design, *Chem. Soc. Rev.*, 2016, **45**(21), 5803–5820, DOI: 10.1039/C6CS00526H.

47 M. J. Frisch, G. W. Trucks, H. B. Schlegel, G. E. Scuseria, M. A. Robb, J. R. Cheeseman, G. Scalmani, V. Barone, G. A. Petersson, H. Nakatsuji, X. Li, M. Caricato, A. V. Marenich, J. Bloino, B. G. Janesko, R. Gomperts, B. Mennucci, H. P. Hratchian, J. V. Ortiz, A. F. Izmaylov, J. L. Sonnenberg, D. Williams-Young, F. Ding, F. Lipparini, F. Egidi, J. Goings, B. Peng, A. Petrone, T. Henderson, D. Ranasinghe, V. G. Zakrzewski, J. Gao, N. Rega, G. Zheng, W. Liang, M. Hada, M. Ehara, K. Toyota, R. Fukuda, J. Hasegawa, M. Ishida, T. Nakajima, Y. Honda, O. Kitao, H. Nakai, T. Vreven, K. Throssell, J. A. Montgomery Jr., J. E. Peralta, F. Ogliaro, M. J. Bearpark, J. J. Heyd, E. N. Brothers, K. N. Kudin, V. N. Staroverov, T. A. Keith, R. Kobayashi, J. Normand, K. Raghavachari, A. P. Rendell, J. C. Burant, S. S. Iyengar, J. Tomasi, M. Cossi, J. M. Millam, M. Klene, C. Adamo, R. Cammi, J. W. Ochterski, R. L. Martin, K. Morokuma, O. Farkas, J. B. Foresman, and D. J. Fox, *Gaussian 16*, Revision A.03, Gaussian, Inc., Wallingford CT, 2016.

48 C. Adamo and V. Barone, Toward reliable density functional methods without adjustable parameters: The PBE0 model, *J. Chem. Phys.*, 1999, **110**, 6158–6170, DOI: 10.1063/1.478522.

49 D. Andrae, U. Häußermann, M. Dolg, H. Stoll and H. Preuß, Energy-adjusted ab initio pseudopotentials for the second and third row transition elements, *Theor. Chim. Acta*, 1990, **77**, 123–141, DOI: 10.1007/BF01114537.

50 W. J. Hehre, R. Ditchfield and J. A. Pople, Self—Consistent Molecular Orbital Methods. XII. Further Extensions of Gaussian—Type Basis Sets for Use in Molecular Orbital Studies of Organic Molecules, *J. Chem. Phys.*, 1972, **56**, 2257–2261, DOI: 10.1063/1.1677527.

51 P. C. Hariharan and J. A. Pople, The influence of polarization functions on molecular orbital hydrogenation energies, *Theor. Chim. Acta*, 1973, **28**, 213–222, DOI: 10.1007/BF00533485.

52 A. V. Marenich, C. J. Cramer and D. G. Truhlar, Universal Solvation Model Based on Solute Electron Density and on a Continuum Model of the Solvent Defined by the Bulk Dielectric Constant and Atomic Surface Tensions, *J. Phys. Chem. B*, 2009, **113**, 6378–6396, DOI: 10.1021/jp810292n.

53 E. C. Meng, T. D. Goddard, E. F. Pettersen, G. S. Couch, Z. J. Pearson, J. H. Morris and T. E. Ferrin, UCSF ChimeraX: Tools for structure building and analysis, *Protein Sci.*, 2023, **32**, e4792, DOI: 10.1002/pro.4792.

54 Pyridine: A Useful Ligand in Transition Metal Complexes | IntechOpen. https://www.intechopen.com/chapters/61452 (accessed 2025-03-15).

55 J. C. Taylor and M. H. Mueller, A Neutron Diffraction Study of Uranyl Nitrate Hexahydrate, *Acta Crystallogr.*, 1965, **19**, 536–543, DOI: **10.1107/S0365110X65003857**.

56 J. M. Haigh and D. A. Thornton, The reaction of ammonia and aliphatic amines with uranyl β-ketoenolates, *J. Inorg. Nucl. Chem.*, 1971, **33**(6), 1787–1797, DOI: **10.1016/0022-1902(71)80616-4**.

57 M. D. Shortridge, D. S. Hage, G. S. Harbison and R. Powers, Estimating Protein–Ligand Binding Affinity Using High-Throughput Screening by NMR, *J. Comb. Chem.*, 2008, **10**(6), 948–958, DOI: **10.1021/cc800122m**.

58 V. Butera, L. D'Anna, S. Rubino, R. Bonsignore, A. Spinello, A. Terenzi and G. Barone, How the Metal Ion Affects the ^{1}H NMR Chemical Shift Values of Schiff Base Metal Complexes: Rationalization by DFT Calculations, *J. Phys. Chem. A*, 2023, **127**(44), 9283–9290, DOI: **10.1021/acs.jpca.3c05653**.

59 M. P. Williamson, Using Chemical Shift Perturbation to Characterise Ligand Binding, *Prog. Nucl. Magn. Reson. Spectrosc.*, 2013, **73**, 1–16, DOI: **10.1016/j.pnmrs.2013.02.001**.

60 E. Faulques, R. E. Russo and D. L. Perry, Raman Studies of Uranyl Nitrate and Its Hydroxy Bridged Dimer, *Spectrochim. Acta, Part A*, 1994, **50**(4), 757–763, DOI: **10.1016/0584-8539(94)80013-8**.

61 H. M. Felmy, N. P. Bessen, H. E. Lackey, S. A. Bryan and A. M. Lines, Quantification of Uranium in Complex Acid Media: Understanding Speciation and Mitigating for Band Shifts, *ACS Omega*, 2023, **8**(44), 41696–41707, DOI: **10.1021/acsomega.3c06007**.

62 H. Wang, S. Y. Sayed, E. J. Luber, B. C. Olsen, S. M. Shirurkar, S. Venkatakrishnan, U. M. Tefashe, A. K. Farquhar, E. S. Smotkin, R. L. McCreery and J. M. Buriak, Redox Flow Batteries: How to Determine Electrochemical Kinetic Parameters, *ACS Nano*, 2020, **14**(3), 2575–2584, DOI: **10.1021/acsnano.0c01281**.

63 E. M. Espinoza, J. A. Clark, J. Soliman, J. B. Derr, M. Morales and V. I. Vullev, Practical Aspects of Cyclic Voltammetry: How to Estimate Reduction Potentials When Irreversibility Prevails, *J. Electrochem. Soc.*, 2019, **166**(5), H3175–H3187, DOI: **10.1149/2.0241905jes**.

64 G. E. Dobereiner and R. H. Crabtree, Dehydrogenation as a Substrate-Activating Strategy in Homogeneous Transition-Metal Catalysis, *Chem. Rev.*, 2010, **110**(2), 681–703, DOI: **10.1021/cr900202j**.

65 A.-F. Voica, A. Mendoza, W. R. Gutekunst, J. O. Fraga and P. S. Baran, Guided Desaturation of Unactivated Aliphatics, *Nat. Chem.*, 2012, **4**(8), 629–635, DOI: **10.1038/nchem.1385**.

66 H. B. Gray, Powering the Planet with Solar Fuel, *Nat. Chem.*, 2009, **1**(1), 7–7, DOI: **10.1038/nchem.141**.

67 K. Arumugam and N. A. Burton, Disproportionation of the Uranyl(V) Coordination Complexes in Aqueous Solution through Outer-Sphere Electron Transfer, *Inorg. Chem.*, 2021, **60**(24), 18832–18842, DOI: **10.1021/acs.inorgchem.1c02575**.

68 D. M. H. Kern and E. F. Orlemann, The Potential of the Uranium(V), Uranium(VI) Couple and the Kinetics of Uranium (v) Disproportionation in Perchlorate Media, *J. Am. Chem. Soc.*, 1949, **71**(6), 2102–2106, DOI: **10.1021/ja01174a055**.

69 M. D. Tzirakis, I. N. Lykakis and M. Orfanopoulos, Decatungstate as an Efficient Photocatalyst in Organic Chemistry, *Chem. Soc. Rev.*, 2009, **38**(9), 2609, DOI: **10.1039/b812100c**.

70 V. D. Waele, O. Poizat, M. Fagnoni, A. Bagno and D. Ravelli, Unraveling the Key Features of the Reactive State of Decatungstate Anion in Hydrogen Atom Transfer (HAT) Photocatalysis, *ACS Catal.*, 2016, **6**(10), 7174–7182, DOI: **10.1021/acscatal.6b01984**.